Electronic Supplementary Material (ESI) for Soft Matter.

Electronic Supplementary Information

Nanoscale adsorbed structures as a robust approach for tailoring polymer film stability

Naisheng Jiang[1], Jiaxun Wang[1], Xiaoyu Di[1], Justin Cheung[2], Wenduo Zeng[1], Maya K. Endoh[1,3], Tadanori Koga[1,2,3,*], Sushil K. Satija[4]

[1]Department of Materials Science and Engineering, Stony Brook University, Stony Brook, New York 11794-2275

[2]Chemical and Molecular Engineering Program, Stony Brook University, Stony Brook, New York 11794-2275

[3]Department of Chemistry, Stony Brook University, Stony Brook, New York 11794-3400

[4]Center for Neutron Research, National Institute of Standards and Technology, Gaithersburg, MD 20899

1. M_w dependent stability of the PS films on the non-treated Si

Fig. S1 shows representative OM images of 3.68kPS, 30kPS, 50kPS and 123kPS single films on the non-treated Si annealed at 150 ºC for 9 days. It is clear that the M_w controlled macroscopic dewetting-to-wetting transition is nearly identical to the PS films on the HF-etched Si described in the main text.

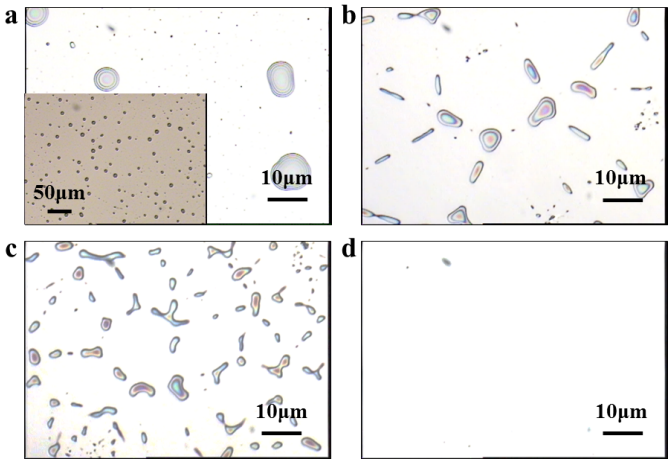

Fig. S1. OM images of the single 20 nm-thick PS films on the non-treated Si after thermal annealing at 150 ºC for 9 days: (a) 3.68kPS; (b) 30kPS; (c) 50kPS; (d) 123kPS. The inset of (a) shows the formation of droplet based cellular patterns with smaller magnification.

2. Surface energy obtained from liquid contact angle measurements

Static contact angle measurements with two liquids (water and glycerol) were carried out using a CAM 200 optical contact angle meter (KSV instruments, Ltd.) equipped with a video camera. A static contact angle (θ) of a film surface was determined on the basis of the three-phase contact line with a 2 μL liquid droplet. All the results were obtained by averaging data from at least 5 individual samples and 10 readings per sample at different locations.

Fig. S2 shows a representative static contact angle of glycerol on the 30kPS flattened layer prepared on the HF-etched Si. It was found that the static contact angles of the flattened layer, the interfacial sublayer, and the 100 nm-thick film are nearly identical (θ = (87 ± 1)° for water and θ = (77 ± 1)° for glycerol, respectively). Therefore, on the basis of the Young's equation ($\gamma_s = \gamma_l \cos\theta + \gamma_{sl}$) and the Owens-Wendt-Kaelble equation ($\gamma_{ls} = \gamma_l + \gamma_s - 2\left(\gamma_s^d \gamma_l^d\right)^{1/2} - 2\left(\gamma_s^p \gamma_l^p\right)^{1/2}$) ($\gamma_s^d$ and γ_s^p are the dispersion and polar parts of the surface energy of the solid, γ_l^d and γ_l^p are the dispersion and polar parts of the surface energy of the liquid)[1], we found that the PS flattened layers and interfacial sublayers have the same surface energy ($\gamma_{PS}^d = 28$ mJ/m^2 and $\gamma_{PS}^p = 4.5$ mJ/m^2) as those of the 100 nm-thick PS film. Note that this value is in line with literature values of surface energy of PS obtained from liquid contact angle measurements[2-4]. We also measured the contact angles of the P2VP layers with the same protocol. The results showed that the P2VP flattened layer, P2VP interfacial sublayer, and 100 nm-thick P2VP film have the same surface energy ($\gamma_{P2VP}^d = 20.25$ mJ/m^2 and $\gamma_{P2VP}^p = 30.25$ mJ/m^2).

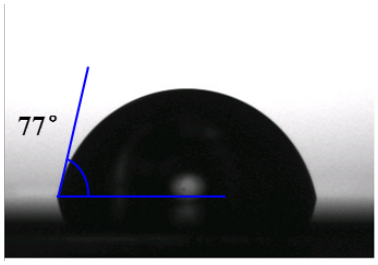

Fig. S2. Static contact angle of glycerol on top of the 30kPS flattened layer prepared on the HF-etched Si.

3. X-ray photoelectron spectroscopy (XPS) results

Fig. S3 shows a representative XPS spectrum of the 30kPS residual layer on the HF-etched Si after toluene leaching. From the figure we can see the prominent peak at a binding of 285.0 eV that is attributed to the C1s peak typically found in hydrocarbons. The discernable peak at a binding energy between 291.0 and 293.0 eV corresponds to the π-π* transition of the phenyl group, as reported previously[5].

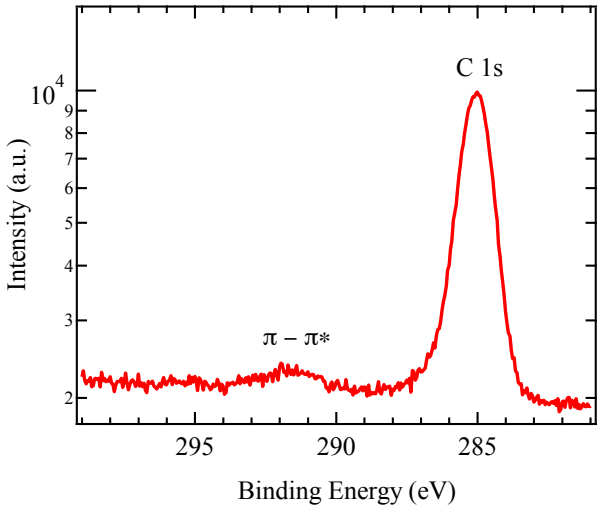

Fig. S3. X-ray photoelectron spectroscopic C 1s narrow scan of the 30kPS flattened layer on the HF-etched Si.

4. Early stage of the dewetting process

Fig. S4 (a) shows the AFM image of the dewetted region of the 30kPS thin film on the H-Si substrate at the early stage of dewetting. The average size of the dewetting holes is still about 1 micron and no coalescence of holes is observed. On the other hand, as shown in Fig. S4 (b), the flattened chains are already formed at the polymer-solid interface, verifying that dewetting takes places on the surface of the flattened layer.

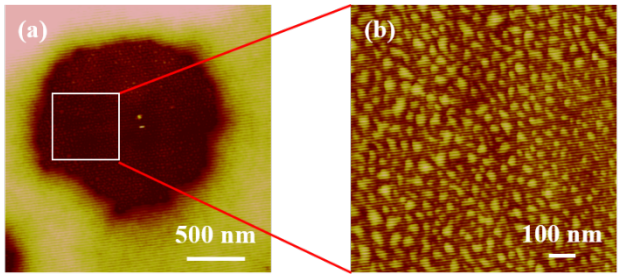

Fig. S4. (a) AFM height image of the 30kPS thin film (20 nm in original thickness) on the H-Si substrate at the early stage of the dewetting process at 150 ºC. The expanded AFM image of the dewetting hole was shown in (b). The height scales for (a) and (b) are 0 – 20 nm and 0 – 10 nm, respectively.

5. Formation of the loosely adsorbed chains

Fig. S5a shows the AFM height image of the residue layer after toluene leaching of the bilayer of the 18 nm-thick 123kPS overlayer and 50kPS flattened layer on the HF-etched Si. Hence, the surface of the residual layer becomes homogeneous compared to the original texture structures shown in Fig. 2b and the thickness was determined to be about 4.0 nm. This indicates the formation of the loosely adsorbed chains during the thermal annealing process for the bilayer. Fig. S5b shows the AFM height image of a bilayer composed of a 123kPS overlayer (18 nm in thickness) on top of the 123kPS flattened layer on the HF-etched Si. The surface morphology of the original 123kPS flattened layer is shown in Fig. S5c. The thickness of the 123kPS flattened layer is estimated to be 2.0 nm ± 0.2 nm based on X-ray reflectivity. The bilayer was annealed at 150 ºC for 9 days and quenched to room temperature. As seen in Fig. S5b, dewetting holes with an average diameter of ≈ 300 nm are seen at the surface. However, we found that these initial holes were formed after an annealing time of less than 1 day and no significant increase in the size was evidenced after subsequent annealing up to 9 days. After the dewetting experiments, we rinsed the bilayer with toluene thoroughly and found that the residue layer was homogenous (≈ 4 nm in thickness), proving that the loosely adsorbed chains were formed via the annealing process and responsible for the prevention of the further hole growth.

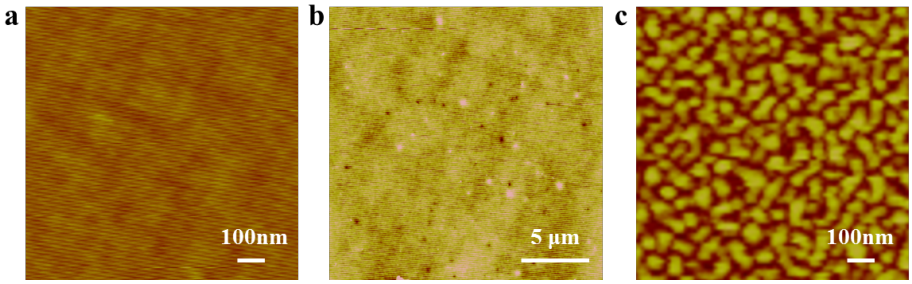

Fig. S5. (a) AFM height image of the residual layer resulting from toluene leaching of the bilayer composed of the 123kPS overlayer on top of the 50kPS flattened layer. (b) AFM height image of the split layer composed of the 123kPS overlayer on top of the 2.0 nm-thick 123kPS flattened layer. The total thickness of the split layer is fixed to 20 nm. The corresponding surface morphology of the 2 nm-thick 123kPS flattened layer on the HF etched Si is shown in (c). The height scales of all the images are 0 – 10 nm. The brightness of the image (b) was tuned to highlight the dewetting holes.

6. Neutron reflectivity (NR) results for the dPS/hPS bilayers

Fig. S6a shows neutron reflectivity (NR) results for the bilayers composed of 4kdPS or 115kdPS overlayers (~ 95 nm in thickness) on top of the 650kPS interfacial sublayer (which consists of the loosely adsorbed chains and flattened chains) after annealing at 150 °C for 24 h. The NR profiles were plotted as a function of the scattering vector in the direction perpendicular to the surface, $q_z = 4\pi sin\theta/\lambda$, where θ is the incident angle and λ is the neutron wavelength (λ = 0.47 nm). As shown in Fig. S6b, we confirmed that the NR profiles for both bilayers do not show significant time evolution after 15 min annealing. To fit the NR data, we used a four layer model: Si (*SLD* = 2.08 × 10^{-4} nm^{-2}), SiOx (*SLD* = 3.47 × 10^{-4} nm^{-2}), the 650kPS interfacial sublayer (*SLD* = 1.42 × 10^{-4} nm^{-2}) and the dPS overlayer (*SLD* = 6.05 × 10^{-4} nm^{-2}). The solid lines correspond to the best-fits to the data based on the volume fraction profiles shown in Fig. 6. Note that the critical evaluation to identify the inner flattened layer is difficult for NR due to the limited q_z value ($q_z < 0.15$ nm^{-1}).

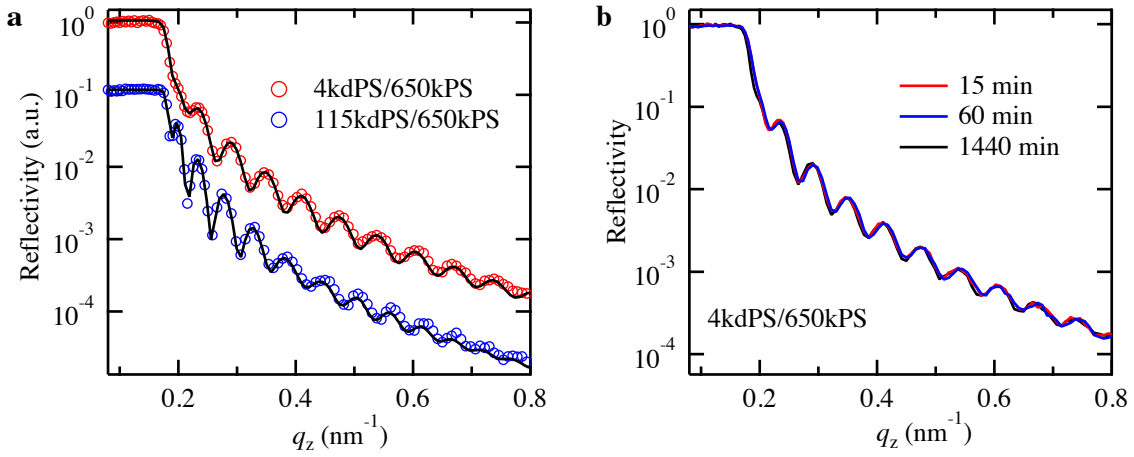

Fig. S6 (a) NR profiles of the bilayers after annealing at 150 °C for 24 h. The solid curves are the best-fits to the data based on the volume fraction profiles shown in Fig. 6 of the main text; (b) Time dependence of the NR profiles for the 4kdPS/650kPS bilayer at 150 °C.

7. Stability of P2VP thin films on the P2VP adsorbed layers

It is known that poly (2-vinylpyridine) (P2VP) has much a stronger affinity to the SiO_x/Si substrate than PS due to the presence of a polar interaction between 2-vinylpyridine segments and hydroxyl groups at the surface of the amorphous SiO_x layer.[6] Here, we used P2VP thin films to illuminate the general roles of the adsorbed chains in film stability of polymer thin films on solids.

Firstly, we focused on the stability of single P2VP films on the SiO_x/Si at $T > T_g$. Single P2VP films (~ 20 nm in thickness) composed of different M_w (M_w = 9 kDa, 36 kDa and 219 kDa, M_w/M_n < 1.11, Scientific Polymer Product Inc., hereafter assigned as 9kP2VP, 36kP2VP, 219kP2VP) were prepared via spin-coating from a dimethylformamide (DMF) solution onto the

non-treated Si and were further annealed at 190 °C under vacuum for prolonged periods of time (up to 2 weeks). Under AFM observation, we found that dewetting holes with the average diameter of ≈ 1 μm formed on the surface of the 9kP2VP film (Fig. S7a). In contrast, both 36kP2VP and 219kP2VP films were stable on the non-treated Si for 2 weeks at 190 °C (Fig. S7b and S7c). The annealed films were then leached with chlorobenzene or DMF to reveal the formation of loosely adsorbed chains and flattened chains on the solid surface, respectively[7]. As a result of XR experiments, we found evidence of the formation of the loosely adsorbed chains in the 36kP2VP and 219kP2VP residue layers (Fig. S8). From the inset of Fig. S8, it can be seen that the 219kP2VP residue layer is also composed of two density layers, similar to what we see in the high M_w PS adsorbed layers shown in the main text (Fig. 4b). However, for the 9kP2VP film, the thickness of the residual layer after the solvent leaching was only ≈ 3 nm (Fig. S8), indicating that only the flattened chains formed on the substrate, similar to the low M_w PS systems described in the main text. Hence, it is reasonable to conclude that even for very strong polymer-solid interactive systems, dewetting may be induced when polymer chains are too short to form loosely adsorbed chains on the substrate. However, in contrast to the low M_w PS films shown in Fig. 1, further development of dewetting of the 9kP2VP film was not evidenced within the experimental time scale. This may be explained by the much stronger solid-segment interaction compared to PS/Si[6], restricting the lateral transportation of the P2VP chains near the substrate. Further experiments are needed for clarification.

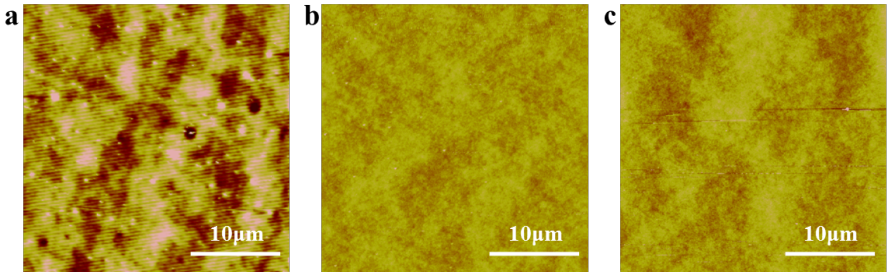

Fig. S7. AFM height images of the 22 nm-thick single films composed of (a) 9kP2VP, (b) 36kP2VP and (c) 219kP2VP deposited on the non-treated Si after annealing at 190 ºC for 5 days. The height scale of the AFM images is 0 – 8 nm. The brightness of the images was tuned to highlight the dewetting holes.

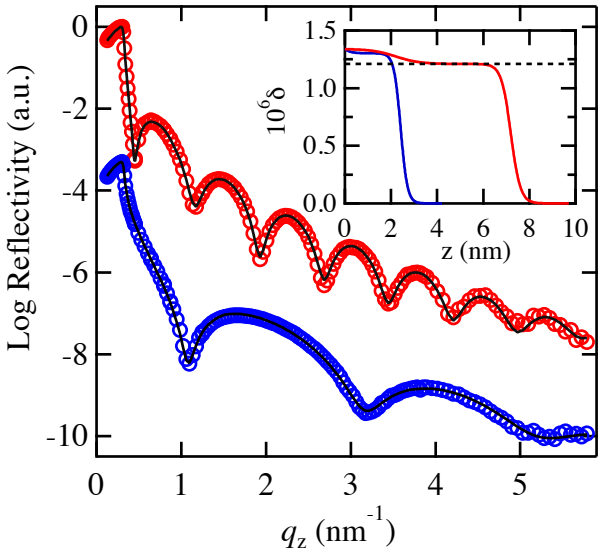

Fig. S8. XR curves of the redisual 219kP2VP layer (red circles) and the redisual 9kP2VP layer (blue circles). The solid lines correspond to the best-fits to the data based on the dispersion (δ) profiles against the distance (z) from the SiO_x surface shown in the inset. Red line: the redisual 219kP2VP layer; blue line: the redisual 9kP2VP layer. The dotted line in the inset corresponds to the δ value of the bulk P2VP.

Secondly, we focused on the roles of the two different P2VP adsorbed chains on the film stability at $T > T_g$ by utilizing split layers. We have previously shown that P2VP adsorbs to the SiO_x/Si substrates, forming the homogeneous flattened layer and interfacial sublayer[7]. To prepare these adsorbed layers, 219kP2VP thin films (≈ 50 nm in thickness) were spin cast from a dimethylformamide (DMF) solution onto the non-treated Si and subsequently annealed at T = 190 °C for up to 10 days under vacuum. The films were then solvent leached in baths of fresh DMF for the flattened layer or chlorobenzene for the interfacial sublayer, respectively. In the same fashion as the PS system, this selective extraction of the two different adsorbed chains is possible due to the large difference in the desorption energy between the outer loosely adsorbed chains and the flattened chains which is proportional to the number of segment-surface contacts[8]. Both solvent leaching conditions were performed at room temperature. The resultant interfacial sublayers and flattened layers were post-annealed at T = 190°C under vacuum overnight to remove any excess solvent. 219kP2VP overlayers on top of the 3 nm-thick 219kP2VP flattened layer or 8 nm-thick interfacial layer with the non-treated Si were prepared via spin-coating from a DMF solution and were further annealed at 190 °C under vacuum for prolonged periods of time (up to 2 weeks). As shown in Fig. S9a, the approximately 20 nm-thick P2VP overlayer ruptured on the P2VP flattened layer, while the same P2VP overlayer remained stable on the P2VP interfacial sublayer (Fig. S9b). Hence, these results were consistent with the film stability of the aforementioned P2VP single layer as well as the findings in the PS/SiO_x/Si system described in the main text: the flattened chains are non-wettable to chemically identical polymer

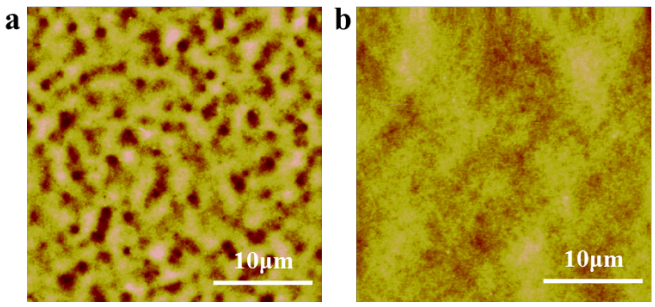

Fig. S9. AFM height images of the 22 nm-thick 219kDa P2VP films deposited on (a) the 3 nm-thick 219kDa P2VP flattened layer and (b) 8 nm-thick 219kDa P2VP interfacial sublayer after annealing at 190 ºC for 8 days. The height scale of the images is 0 – 8 nm, respectively. The brightness of the images were tuned to highlight the dewetting holes.

melt chains, while the loosely adsorbed chains stabilize the film against dewetting. Static liquid contact angle measurements (see the aforementioned section 2) further indicate that the difference in the wettability between the flattened layers and interfacial sublayers is entropically driven.

Fig. S10 (a) summarizes the time evolution of the average radius of the hole (r_h) of a 22 nm-thick 219kDa P2VP overlayer deposited on a 3 nm-thick 219kDa P2VP flattened layer based on the AFM experiments. From the figure we can see that the growth process is classified into two-stages: (i) at $t < 118$ h, the power-law growth ($r_h \sim t^{0.4}$); (ii) the hole growth saturates at around $r_h = 450$ nm and shows a plateau at $t_{an} > 118$ h. In addition, it should be mentioned that there are no visible rims (see, Fig. S9a), characteristic dewetting structures associated with the highly elastic nature of a polymer against the driving capillary force[9], even at the late stage of the kinetics. This can be explained by the fact that the radius of the hole is smaller than the critical size ($R_c = hb$, where h and b are the film thickness of the overlayer and the hydrodynamic extrapolation length, respectively) above which the onset of rims is triggered[10]. The theoretical value of b is given by $b=a(N^3/N_e^2)$, where a is the segment length, N is the degree of polymerization, N_e is the threshold for entanglements. For the present case with the b value of 156 μm, R_e is estimated to be 1.7 μm, which is much larger than the radii of the holes observed in this study. Besides, the depth of the holes from the polymer/air interface is at most 8 nm even at t = 150 h (i.e., the plateau regime), which is still far away from the substrate surface. Furthermore, the power law growth (with the exponent of 0.4) at the early stage suggests that the dewetting process is governed by slippage[11], while the exponent is slightly smaller than the theoretical value (2/3) for hole-growth with strong slip[10, 11]. Hence, it is clear that the overall dewetting kinetics (including the size of the holes and the exponent of the power-law growth) is significantly retarded compared to typical polymer dewetting on non-wettable solid substrates.

In order to further discuss the origin of the suppressed dewetting dynamics and highlight the correlation with the nanoscale interface structures, we rinsed the dewetted bilayers with chlorobenzene that enabled us to extract the P2VP loosely adsorbed chains (if any)[7]. Fig. S10 (b) shows the thickness of the 219kDa P2VP residue layers after the solvent leaching and subsequent drying at 190 °C for 12 h measured by XR. From the figure we can see that the thickness of the residual layer remained nearly constant (~ 3 nm) at the early stage (t < 10 h). This thickness is equivalent to the thickness of the original flattened layer. On the other hand, at t > 10 h, the thickness of the residual layer increases with increasing the annealing time, demonstrating that the free chains in the top P2VP film start to "reel-in" the empty space of the flattened layer[7], causing the formation of the loosely adsorbed chains (i.e., the connectors). The link between Fig. S10 (a) and (b) illuminates the strong correlation between the hindrance of dewetting and the growth of the connectors, similar to those found in the PS systems described in the main text.

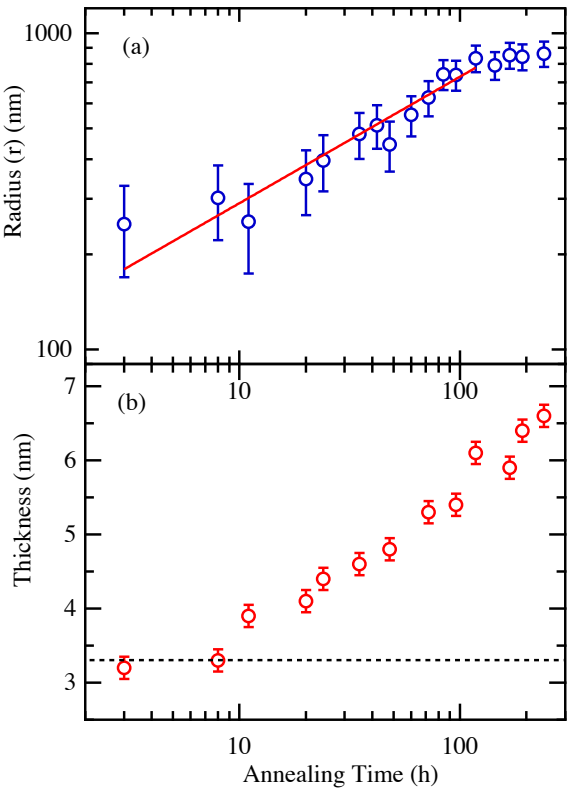

Fig. S10. (a) Change in radius of dewetting holes (r_h) of 22 nm-thick 219kDa P2VP films on P2VP flattened layer as a function of annealing time (t) at 190 ºC. The dotted lines correspond to the power-law growth ($r_h \sim t^{0.4}$) at the early stage (at t < 118 h) and the plateau at the later stage (t > 118 h). (b) Change in the residual thickness of the 22 nm thick P2VP film deposited on P2VP 3 nm-thick equilibrium flattened layer after leaching by chlorobenzene as a function of t.

References

1. Kwok, D. Y.; Neumann, A. W. Adv. Colloid Interfac. **1999**, 81, 167-249.
2. Omenyi, S. N.; Neumann, A. W.; van Oss, C. J. *J. Appl. Phys.* **1981,** 52, (2), 789-795.
3. Kwok, D.; Neumann, A.; Mittal, In *Acid-base Interactions: Relevance to Adhesion Science and Technology*, Vol 2, K. *Mittal, KL, Ed* **2000**.
4. Kwok, D. Y.; Lam, C. N. C.; Li, A.; Zhu, K.; Wu, R.; Neumann, A. W. *Polym. Eng. Sci.* **1998,** 38, (10), 1675-1684.
5. Fujii, Y.; Yang, Z. H.; Leach, J.; Atarashi, H.; Tanaka, K.; Tsui, O. K. C. *Macromolecules* **2009**, 42, 7418-7422.
6. vanZanten, J. H.; Wallace, W. E.; Wu, W. L. *Phys. Rev. E* **1996**, 53, R2053-R2056.

7. Jiang, N.; Shang, J.; Di, X.; Endoh, M. K.; Koga, T. *Macromolecules* 2014, 47, 2682-2689.
8. O'Shaughnessy, B.; Vavylonis, D. *Phys. Rev. Lett.* **2003**, 90, 056103.
9. Reiter, G. *Phys. Rev. Lett.* **2001**, 87, 186101.
10. Brochard-Wyart, F.; Debregeas, G.; Fondecave, R.; Martin, P. *Macromolecules* **1997**, 30, 1211-1213.
11. Reiter, G.; Khanna, R. *Langmuir* **2000**, 16, 6351-6357.